Use of a Glutaric Acid Cocrystal to Improve Oral Bioavailability of a Low Solubility API

ARTICLE *in* PHARMACEUTICAL RESEARCH · SEPTEMBER 2006

Impact Factor: 3.42 · DOI: 10.1007/s11095-006-9032-3 · Source: PubMed

9 AUTHORS, INCLUDING:

Daniel Mcnamara
Bristol-Myers Squibb
5 PUBLICATIONS **399** CITATIONS
SEE PROFILE

Manjunath S Shet
Purdue Pharma L.P.
40 PUBLICATIONS **1,403** CITATIONS
SEE PROFILE

Aeri Park
Almac
9 PUBLICATIONS **810** CITATIONS
SEE PROFILE

Pharmaceutical Research, Vol. 23, No. 8, August 2006 (© 2006)
DOI: 10.1007/s11095-006-9032-3

Research Paper

Use of a Glutaric Acid Cocrystal to Improve Oral Bioavailability of a Low Solubility API

Daniel P. McNamara,[1,4] Scott L. Childs,[2,3] Jennifer Giordano,[1] Anthony Iarriccio,[1] James Cassidy,[1] Manjunath S. Shet,[1] Richard Mannion,[1] Ed O'Donnell,[1] and Aeri Park[2]

Received September 29, 2005; accepted April 10, 2006

Purpose. The bioavailability of a development candidate active pharmaceutical ingredient (API) was very low after oral dosing in dogs. In order to improve bioavailability, we sought to increase the dissolution rate of the solid form of the API. When traditional methods of forming salts and amorphous material failed to produce a viable solid form for continued development, we turned to the non-traditional approach of cocrystallization.
Methods. A crystal engineering approach was used to design and execute a cocrystal screen of the API. Hydrogen bonding between the API and pharmaceutically acceptable carboxylic acids was identified as a viable synthon for associating multiple components in the solid state. A number of carboxylic acid guest molecules were tested for cocrystal formation with the API.
Results. A cocrystal containing the API and glutaric acid in a 1:1 molecular ratio was identified and the single crystal structure is reported. Physical characterization of the cocrystal showed that it is unique regarding thermal, spectroscopic, X-ray, and dissolution properties. The cocrystal solid is nonhygroscopic, and chemically and physically stable to thermal stress. Use of the cocrystal increased the aqueous dissolution rate by 18 times as compared to the homomeric crystalline form of the drug. Single dose dog exposure studies confirmed that the cocrystal increased plasma AUC values by three times at two different dose levels.
Conclusions. APIs that are non-ionizable or demonstrate poor salt forming ability traditionally present few opportunities for creating crystalline solid forms with desired physical properties. Cocrystals are an additional class of crystalline solid that can provide options for improved properties. In this case, a crystalline molecular complex of glutaric acid and an API was identified and used to demonstrate an improvement in the oral bioavailability of the API in dogs.

KEY WORDS: bioavailability; cocrystal; crystal engineering; intrinsic dissolution rate; pharmacokinetics; solubility.

INTRODUCTION

This manuscript describes the discovery, physico-chemical characterization, and *in vivo* proof of efficacy of a glutaric acid cocrystal of a low solubility development candidate active pharmaceutical ingredient (API). 2-[4-(4-chloro-2-fluorophenoxy)phenyl]pyrimidine-4-carboxamide (**1**), belongs to the pharmacologic class of sodium channel blockers and was developed as a potential drug candidate useful for treating or preventing surgical, chronic and neuropathic pain (Fig. 1). Compound **1** possesses extremely low solubility characteristics (<0.1 μg/ml) in aqueous systems. Although the permeability of **1** could not be measured in Caco-2 cells because of its inherently low solubility, **1** is suspected to be a Class II compound (low solubility and high permeability) as described in the biopharmaceutical drug classification scheme (BCS) (1). The calculated octanol/water partition coefficient (clogP) for **1** is 2.9 (2), supporting this suspicion (3). As expected with Class II BCS compounds, **1** showed low *in vitro* dissolution and low *in vivo* plasma concentrations after oral dosing of the crystalline solid in dogs.

In order to increase bioavailability we examined the potential of forming cocrystals, or crystalline molecular complexes, of **1** with the specific intention of increasing the dissolution rate. The use of cocrystallization as a tool to improve the pharmaceutical properties of solid drug candidates is a subject that has seen increasing application in the literature (4–6). With an appropriate pairing of host and guest, hydrogen bonding promotes formation of a stable crystalline complex that contains both API and the secondary non-toxic guest molecule in a stoichiometric ratio (7).

During development of non-ionizable or poor salt-forming APIs, there are few options for generating faster dissolving more soluble crystalline forms. Meta-stable poly-

[1] Purdue Pharma L. P., 444 Saw Mill River Road, Ardsley, New York 10502, USA.
[2] SSCI Inc., West Lafayette, Indiana 47906, USA.
[3] Design Science Research, Atlanta, Georgia 30306, USA.
[4] To whom correspondence should be addressed. (e-mail: daniel.mcnamara@pharma.com)

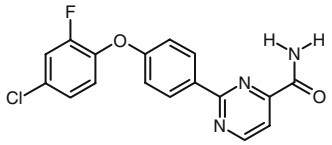

Fig. 1. 2-[4-(4-chloro-2-fluorophenoxy)phenyl]pyrimidine-4-carboxamide (**1**).

morphs, solvates, or hydrates are typically the only other crystalline forms that are pursued; however, it has been shown that APIs can form molecular complexes with other small molecules (8–11). These cocrystals may have unique physical properties such as improved dissolution rate and, as long as the second component (the guest compound) is suitably non-toxic, the cocrystal can be considered a pharmaceutically acceptable solid for dosage form development.

Cocrystallization should not be confused with other techniques in which an API is processed in the presence of an additional molecular species in order to produce a material with desirable physical properties. While it is conceivable that **1** and glutaric acid could form a product by coprecipitation, eutectic formation, or in a solid solution or dispersion, these processes are distinctly different from cocrystallization as we have defined it.

Cocrystal discovery relies on applying crystal engineering techniques that have become well developed over the last two decades (12–18). Formation of a molecular complex of an API and a second molecule typically requires complementary hydrogen bonding between the two components. In this case, access to the best hydrogen bond accepting sites, the aromatic nitrogen bases, are hindered by the proximity of C–H groups on the neighboring co-planar phenyl ring. Thus, the most useful hydrogen bonding group is the amide functionality, which is known to form robust hydrogen bond interactions with un-ionized carboxylic acids (19–21). Non-toxic carboxylic acids normally used in salt screens were used in this case to screen for cocrystals of **1**.

The crystal engineering techniques used to design and execute the cocrystal screen of **1** are described. This approach resulted in the discovery of a cocrystal with a 1:1 stoichiometric ratio of **1** and glutaric acid as a potentially viable solid crystalline form of **1**. The glutaric acid cocrystal (**2**) showed an 18 times greater intrinsic dissolution rate and three times the plasma area-under-the-curve (AUC) as compared to **1** in a single dose dog exposure study. The improved *in vivo* exposure gained through use of the cocrystal is the first time that a cocrystal has been reported to improve the bioavailability of an API as compared to dosing the parent compound. Cocrystal **2** was also shown to be chemically and physically stable for storage under stress conditions of 40°C/75% relative humidity (RH) and 60°C for 2 months.

MATERIALS AND METHODS

Physico-Chemical Characterization of Parent Compound 1 and Cocrystal 2

Differential scanning calorimetry (DSC) was performed with a PerkinElmer, Pyris 1 DSC. Each DSC sample was sealed in a 50 μl aluminum pan with a pierced lid and heated through the respective melting temperatures at scan rates of 10°C/min. Modulated DSC was performed with a TA Instruments 2920 DSC. The amorphous glass of **1** was prepared by heating at 10°C/min to 220°C and then quickly cooling to −50°C. The glass was then heated using a modulation amplitude of ±0.80°C and a 60 s period with an underlying heating rate of 1°C/min from 25 through 100°C. X-ray powder diffraction (XRPD) patterns were collected on a Philips Analytical X'Pert Plus MPD X-ray diffractometer using a Cu tube at 50 kV and 40 mA. The scan range was 4–40°2θ with a step size of 0.02°2θ/s and the time per step of 1 s. A Surface Measurement Systems DVS-1000 was used for dynamic water sorption characterization. The sample was dried under nitrogen at 0% RH, 25°C until the sample met equilibration conditions of less than 0.0001% weight change. The sample was cycled twice in 5% RH steps from 0 through 95% RH.

To analyze the cocrystal under a humidity challenge, a VTI RH 200 Relative Humidity Generator was attached to the XRPD sample stage. The humidity generator was set to 100% RH and to ensure 100% RH inside the sample chamber, a vial of open water was also placed in the sample chamber. XRPD was performed at room temperature after 2, 6, and 24 h exposure to 100% RH.

Cocrystal Screening

Thermal microscopy methods were used to determine if a particular carboxylic acid was able to cocrystallize with **1** using melt or highly saturated solution conditions. A total of 26 carboxylic acids were screened using a binary-melt technique on a microscope slide. In this procedure, often referred to as the Kofler technique, two compounds are melted adjacent to one another and mixed by application of a coverslip. At the interface where the compounds mix, a molecular complex containing both components may form under appropriate conditions. High boiling organic liquids such as methyl salicylate or methyl benzoate were used to create highly concentrated solutions in which the melting point of the API was reduced. By varying the liquid composition and concentration of each component before they were mixed, the conditions of an individual experiment could be tailored to match the particular guest being tested. A positive interaction was determined visually by observing the slide through crossed polarizing filters. In a negative interaction, the mixing of the guest and **1** created a eutectic where no crystallization occurred while a positive interaction produced crystalline material at the binary interface. The products were analyzed by Raman spectroscopy. Five unique cocrystals were identified using this technique. Thermal microscopic images were acquired using transmitted light and crossed polarizers on a microscope stage with temperature control.

Synthesis of Glutaric Acid Cocrystal (2) by Solution Methods

Compound **1** (2.898 g, 8.431 mmol) and glutaric acid (Sigma-Aldrich Co., 1.111 g, 8.410 mmol) were dissolved in 150 ml of boiling chloroform with stirring. The solution was concentrated by continued boiling until the volume was

Table I. Crystal Data and Structure Refinement for **2**

Identification code	a39g337s
Empirical formula	C22 H19 Cl F N3 O6
Formula weight	475.85
Temperature	173(2) K
Wavelength	1.54178 Å
Crystal system	Monoclinic
Space group	P2(1)/n
Unit cell dimensions	a = 15.8957(5) Å α = 90°. b = 5.3079(2) Å β = 97.963(2)°. c = 25.5345(8) Å γ = 90°.
Volume	2,133.64(12) $Å^3$
Z	4
Density (calculated)	1.481 Mg/m^3
Absorption coefficient	2.076 mm^{-1}
F(000)	984
Crystal size	0.14 × 0.12 × 0.07 mm^3
Theta range for data collection	3.09 to 67.50°
Index ranges	-17 < = h < = 18, -6 < = k < = 6, -30 < = l < = 26
Reflections collected	10,017
Independent reflections	3625 [R(int) = 0.0524]
Completeness to theta = 67.50°	94.2%
Absorption correction	Semi-empirical from equivalents
Max. and min. transmission	0.8683 and 0.7599
Refinement method	Full-matrix least-squares on F^2
Data/restraints/parameters	3625/0/314
Goodness-of-fit on F^2	1.071
Final R indices [I > 2sigma(I)]	R1 = 0.0562, wR2 = 0.1340
R indices (all data)	R1 = 0.0749, wR2 = 0.1417
Largest diff. peak and hole	0.282 and -0.276 e.$Å^{-3}$

50 ml. Seeds of the cocrystal generated in thermal experiments or from previous batches were introduced to the hot solution (in our hands, spontaneous nucleation under these conditions always resulted in the stable form of **1**). Crystallization occurred rapidly and was allowed to proceed as the solution cooled over approximately 15 min. Approximately 100 ml of cyclohexane were added and the resulting solution was cooled on ice for 30 min. Cocrystal **2** was isolated by filtration and allowed to dry in the air (3.705 g, 92% yield). A single crystal was isolated from the recovered product and used in the single crystal X-ray diffraction study.

Raman Spectroscopy

Raman spectra were collected with a Chromex Sentinel dispersive Raman unit equipped with a 785 nm, 70 mW excitation laser and a TE cooled CCD (1024 × 256 pixels, < 0.1e-/pixel/sec). A fiber-optically coupled filtering probe was used to collect data in the spectral range 125 to 2,180 cm^{-1} at a resolution of 4 cm^{-1}. Each spectrum is a result of two co-added 20 s scans. The unit has continuous automatic calibration using an internal standard. The data were collected by SentinelSoft data acquisition software and processed in GRAMS/AI V.7.

Single Crystal X-ray Diffraction (SCXRD)

A suitable crystal of **2** was coated with Paratone N oil, suspended in a small fiber loop and placed in a cooled nitrogen gas stream at 100 K on a Bruker D8 SMART 1000 CCD sealed tube diffractometer with graphite monochro-

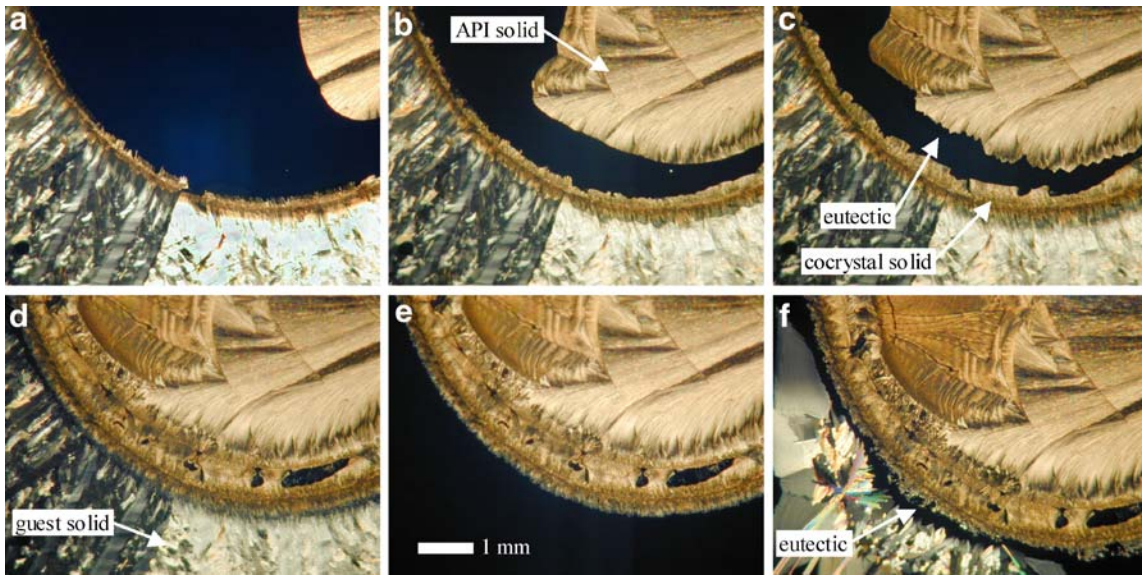

Fig. 2. Cocrystal screening using the Kofler technique is shown in this series of micrographs. Glutaric acid (located in the *bottom half of images*) and the API (*top half of images*) are dissolved in a high boiling solvent on a microscope slide. The interface where the two compounds mix is where cocrystal formation occurs. Crystal growth is manipulated by adjusting the temperature. In (a), (b), and (c) the cocrystal (*curved line in center*) is growing at the boundary of the glutaric acid domain. The *dark area* (liquid phase as viewed through crossed polarizers) is a eutectic that separates the cocrystal from the API. When the components mix, the concentrations vary across the slide and colligative properties cause a melting point depression effect. A eutectic will also form between glutaric acid and the cocrystal. In (d) a *narrow* eutectic forms as the temperature approaches the melting point of glutaric acid. In (e) the glutaric acid has completely melted, clearly showing the boundary of the cocrystal solid phase. When the temperature is lowered again in (f), the glutaric acid grows in and forms a clean eutectic with the cocrystal phase.

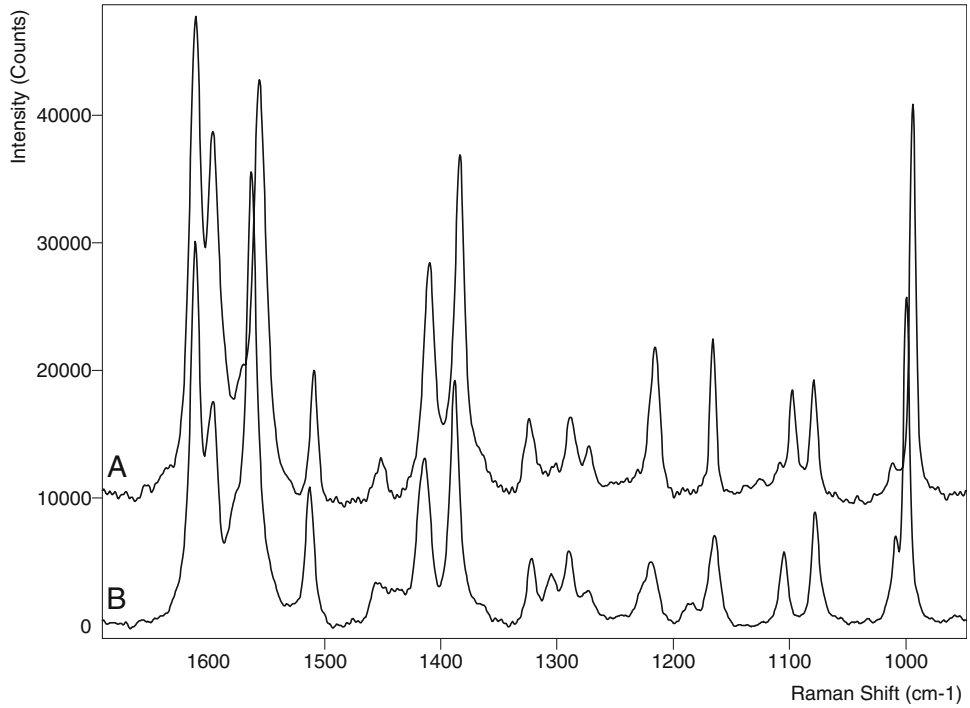

Fig. 3. Fingerprint region of Raman spectra of **1** (A) and **2** (B).

mated CuK_α (1.54178 Å) radiation. Data were measured using a series of combinations of phi and omega scans with 10-s frame exposures and 0.3° frame widths. Data collection, indexing and initial cell refinements were all carried out using SMART software (22). Frame integration and final cell refinements were done using SAINT software (23). The final cell parameters were determined from least-squares refinement on 3625 reflections. The structure was solved using Direct methods and difference Fourier techniques (SHELXTL, V5.10) (24). All the hydrogen atoms were located from difference Fouriers and included in the final cycles of least squares with isotropic U_{ij}'s. All non-hydrogen atoms were refined anisotropically. Scattering factors and anomalous dispersion corrections are taken from the *International Tables for X-ray Crystallography* (25). Structure solution, refinement, graphics and generation of publication materials were performed by using SHELXTL, V5.10 software. Additional details of data collection and structure refinement are given in Table I.

Chemical and Physical Stability of 2

Samples of cocrystal **2** were placed in glass bottles at 40°C/75% RH and 60°C and tested periodically during 2-months storage. Samples were tested by XRPD, DSC, and assayed for impurities using a high performance liquid chromatography technique with ultraviolet detection (HPLC-UV) method.

Intrinsic Dissolution Studies

Intrinsic dissolution measurements were performed using a fiber optic probe (Delphian® type IIA fiber optic workstation, baseline correction mode with sample wavelength maximum of 279 nm and baseline wavelength of 350 nm) at 37°C and 100 rpm in a USP apparatus II dissolution vessel (Vankel VK7010) containing 500 ml of pure water. Disks 0.8 cm diameter were compressed using 70 mg of solid in stainless steel dies (Vankel Woods apparatus) at 1,000 lbs for 60 s with a Carver Press. Dissolution studies for cocrystal **2** lasted 90 min, after which time the disks were recovered, carefully ground and checked by XRPD for the presence of cocrystal. The solubility of **1** is so low that dissolution studies were run over 24 h in order to get a measurable rate.

Pharmacokinetic Evaluation

A study was conducted to compare the pharmacokinetic profiles of **1** and **2**. Compounds **1** and **2** were administered as

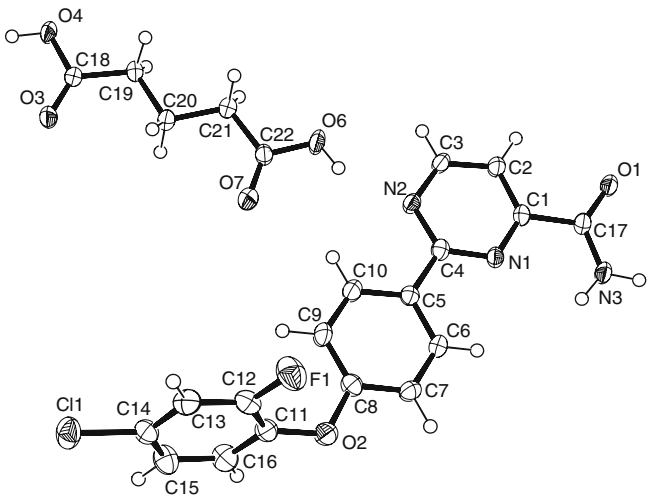

Fig. 4. ORTEP drawing (ellipsoids at 50% probability level) of the glutaric acid cocrystal (**2**).

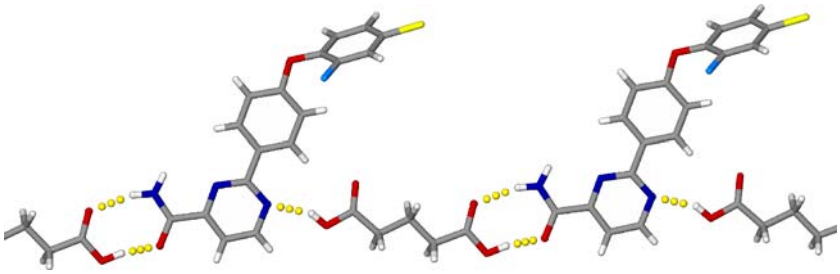

Fig. 5. Hydrogen bonding in **2** consists of interactions between the carboxylic acid groups of the glutaric acid molecule and the amide and pyridine groups on the drug molecule.

neat solids to six male beagle dogs in a crossover study with a 2-week washout period between treatments. Each dog was dosed with either **1** or **2** in a gelatin capsule after an overnight fast. All research involving animal subjects adhered to the "Principles of Laboratory Animal Care" (NIH publication #85-23). Dose levels of 5 and 50 mg/kg were each evaluated. Each dog received one size #2 capsule for the 5 mg/kg dose. Dosing at 50 mg/kg required use of two size #00 capsules for each dog. Blood samples were collected at intervals for 36 h post-dose. Non-compartmental pharmacokinetic metrics were determined using WinNonlin v. 1.5 (Scientific Consulting, Inc., Mountain View, CA). The area under the plasma concentration-time curve (AUC) was estimated by application of the linear trapezoidal rule. Statistical analyses were conducted using Microsoft Excel 2000; statistical significance was considered when $p < 0.05$.

Particle Size Evaluation

Particle size of each of the lots of **1** and **2** dosed in the pharmacokinetic studies were characterized using an instrumented light scattering particle sizer (Malvern 2000). Samples from each lot were suspended in Millipore deionized water with 5 drops of Triton X-100 in 2 l included as a dispersant. Samples were analyzed in the particle-in-liquid mode.

RESULTS AND DISCUSSION

Compound **1** is poorly soluble in water, with measured values of less than 0.1 μg/ml in pure water, SGF (simulated gastric fluid), and SIF (simulated intestinal fluid). Solubility in fed state SIF (FeSSIF), which contains the surfactants taurocholate and lecithin, was improved at 14 μg/ml. Attempts to use other more lipophilic pharmaceutical vehicles such as propylene glycols and Cremophors did not increase the solubility of **1** sufficiently to allow these approaches to be of practical utility during subsequent exposure studies.

Compound **1** is a weak base and was not amenable to typical acid salt formation with hydrochloric, sulfuric, phosphoric or other typical pharmaceutically acceptable, strong acids. The estimated p*K*a of the conjugate acid of **1** is −0.7 (2). As expected, **1** is such a weak base that solubility in SGF (pH 1.2) was comparable to neutral water and SIF (pH 6.5). Attempts to make amorphous **1** using the typical techniques of milling or solvent evaporation of organic solutions were

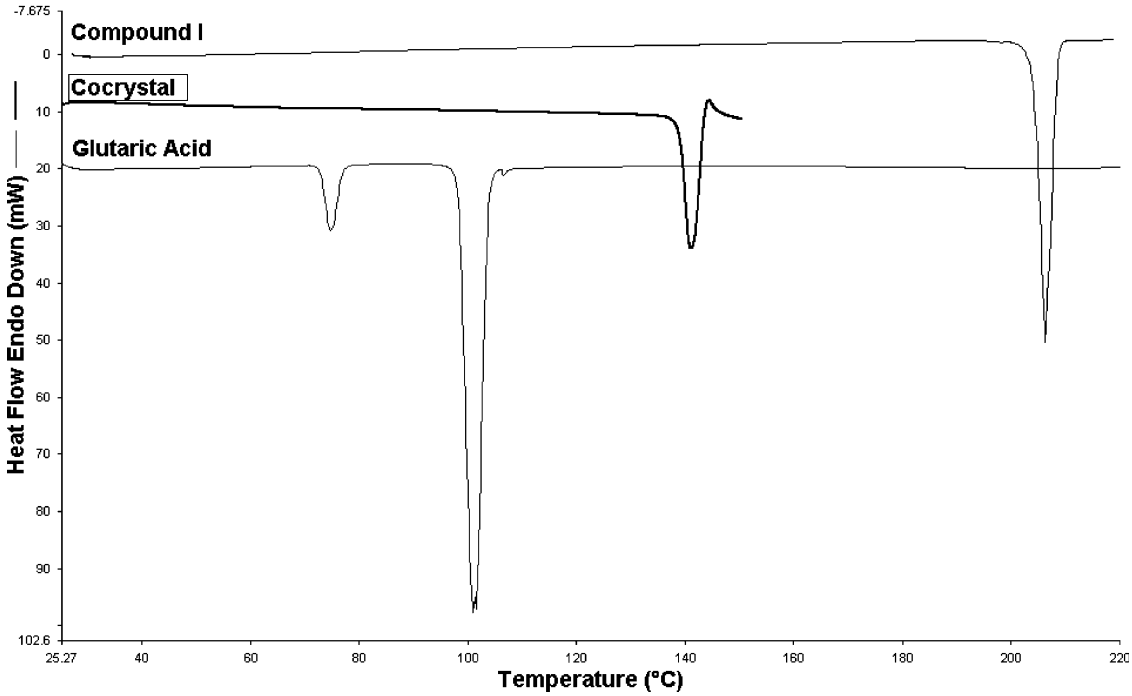

Fig. 6. DSC Scans of **1**, **2**, and glutaric acid.

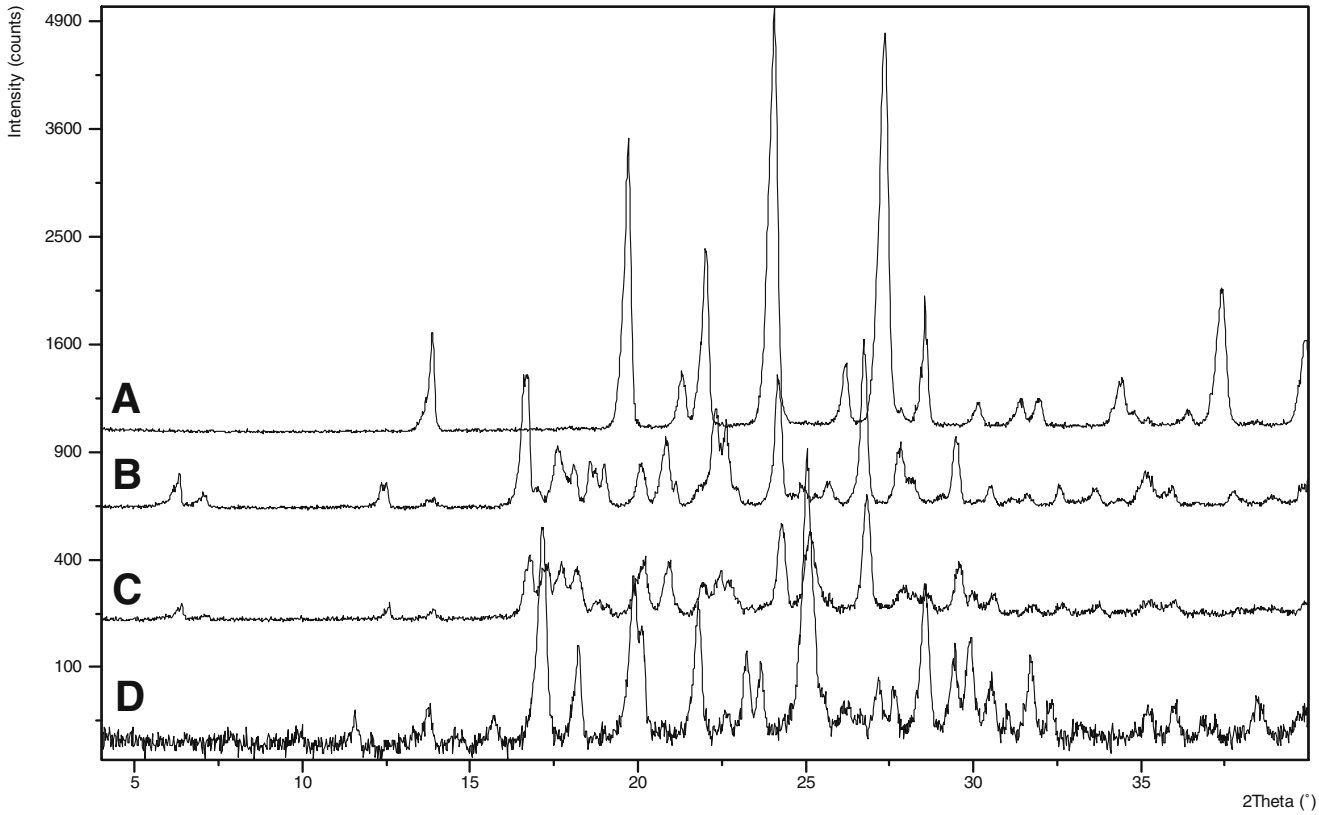

Fig. 7. XRPD of glutaric acid (A); **2** (B); **2** after dissolution testing (C); **1** (D).

also not successful. Further investigation using modulated DSC showed that the glass transition temperature (Tg) of **1** is about 43°C. Given that the Tg is so close to room temperature, it is not surprising that amorphous **1** could not be routinely made at room temperature. Further, we did not favor use of amorphous **1** in dosage form development because crystallization would likely appreciably limit the expiry period or shelf life of a dosage form containing such a metastable solid. Since the usual pharmaceutical tactics of salt formation or use of an amorphous phase were not amenable for **1**, the non-traditional approach of cocrystal formation was employed.

A set of 26 pharmaceutically acceptable carboxylic acids commonly used in salt screening studies (26) were selected as potential cocrystal guest compounds. Solutions of **1** and guest acids resulted in the API crystallizing from solution in nearly all cases when crystallization occurred because **1** has lower solubility than the carboxylic acid guests in almost all solvents. Because of this solubility limitation, we choose to use a cocrystal screening technique based on the Kofler (27–29) method. This technique uses binary melt experiments performed on a microscope hotstage. Cocrystals formed at the interface of the two components (Fig. 2) (30,31).

Five new solid phases were identified using the Kofler method and were confirmed to be cocrystals by Raman spectroscopy (Fig. 3). Of these five, the glutaric acid cocrystal (**2**) was selected as the development candidate because its melting point suggested that it would be stable during storage and the high water solubility of glutaric acid guest was expected to contribute to an increased dissolution rate in water. In addition to being a natural component of dietary foodstuffs, glutaric acid is a normal metabolic intermediate of fatty acid, tryptophan, and lysine metabolism. Cocrystal **2** contains **1** and glutaric acid in a 1:1 molar ratio, which corresponds to 72 wt.% of **1**, a loading volume that was acceptable.

Development of a procedure to prepare **2** in gram quantities proved to be non-trivial. Initial experiments using a 1:1 molar ratio of the components in a variety of solvents yielded only **1** or mixtures of **1** and glutaric acid as the products. The successful method is a kinetic crystallization from chloroform, with control of nucleation by seeding.

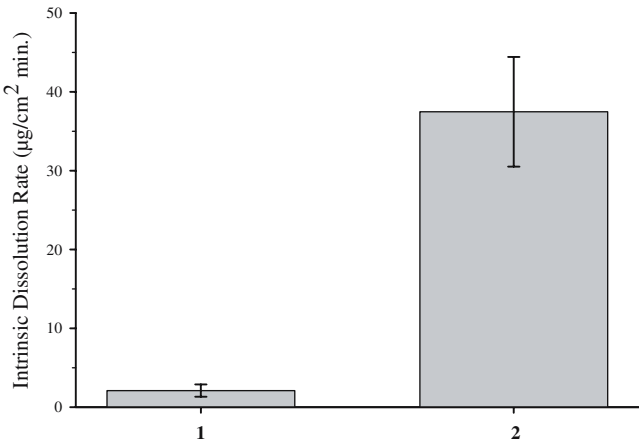

Fig. 8. Intrinsic dissolution rate of **1** and **2** at 100 rpm 37°C in pure water (*error bars* show standard deviations, $n = 3$, ANOVA for means with unequal variances, $p = 0.0119$).

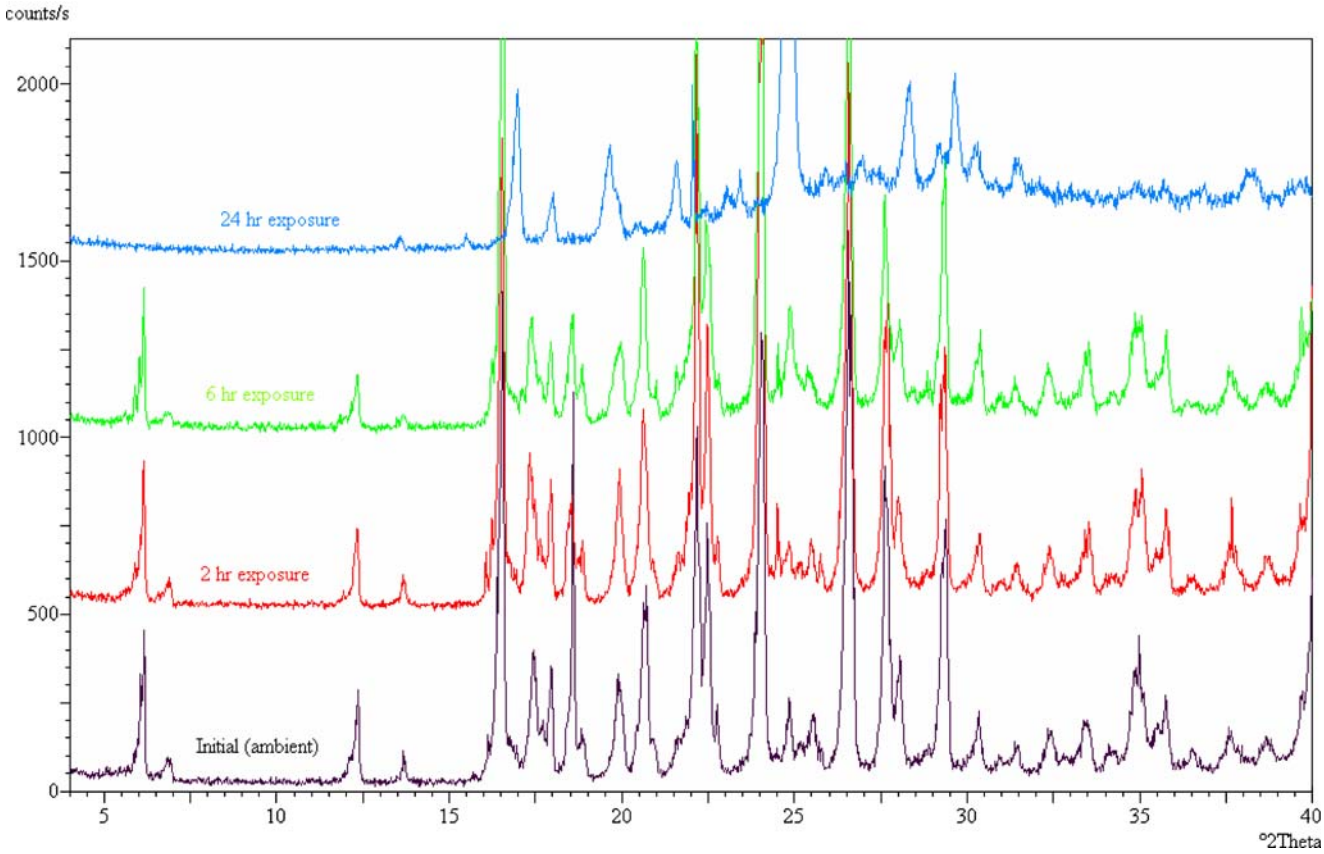

Fig. 9. XRPD of **2** with exposure to 100% RH at room temperature.

Without seeding, nucleation of **1** was observed from solution under all conditions and solvent systems tested.

The single crystal X-ray data for **2** are summarized in Table I. One carboxylic acid group of glutaric acid hydrogen bonds to the amide functionality in a self-complementary eight membered ring motif (Figs. 4 and 5). The second acid group forms an unexpected interaction with a pyrimidine acceptor site. The approach of the acid hydrogen bond donor to the pyrimidine nitrogen is sterically hindered and results in a relatively long H to N distance of 1.96 Å and O–H·N angle of 152°.

DSC experiments indicated that **1** melts at 206°C and that **2** melts at 142°C. Glutaric acid undergoes a solid–solid transformation near 75°C to a phase that melts at 97.5°C (32). The DSC scans are shown in Fig. 6. The cocrystal (**2**) exhibits a unique XRPD pattern that allows it to be distinguished from **1** and glutaric acid (Fig. 7).

Results of the intrinsic dissolution comparison of **1** and **2** are shown in Fig. 8. The cocrystal shows a statistically significant improvement in dissolution rate of approximately 18 times that of **1** in water at 37°C. Disks of **2** which were used in the dissolution study were patted dry with a tissue and ground slightly and then examined by XRPD after 90 min in the dissolution bath. The XRPD patterns in Fig. 7 show that solid recovered after 90 min contact with liquid water from the intrinsic dissolution study is still primarily **2**. Some small peaks from the recovered solid sample are consistent with the presence of small amounts of **1**. However, it appears that the

Table II. Comparison of Mean Pharmacokinetic Parameters for **1** and Glutaric Acid Cocrystal

Dose Group	T_{max} (hr)	C_{max} (ng/mL)	AUC (ng hr/mL)
5 mg/kg **1**	13 ± 12	25.4 ± 11.4	374 ± 192
5 mg/kg Cocrystal	6 ± 9	89.2 ± 57.7	1,234 ± 613
50 mg/kg **1**	13 ± 14	89.2 ± 68.7	889 ± 740
50 mg/kg Cocrystal	2 ± 0	278 ± 70.5	2,230 ± 824

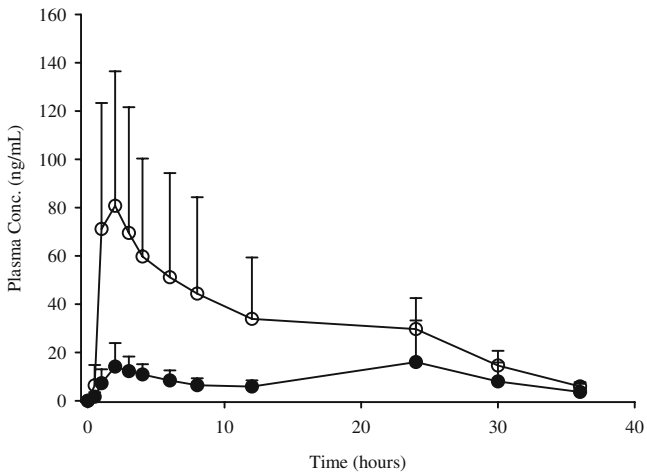

Fig. 10. Dog plasma concentration with time for 5 mg/kg dosing of **1** (*solid circles*) and **2** (*open circles*). *Error bars* show +1 standard deviation.

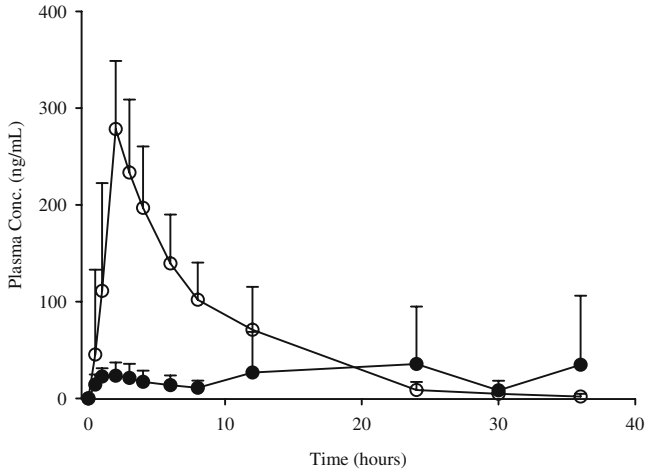

Fig. 11. Dog plasma concentration with time for 50 mg/kg dosing of **1** (*solid circles*) and **2** (*open circles*). *Error bars* show +1 standard deviation.

dissolution results were not skewed by gross solid phase transformation during the course of the 90 min dissolution experiment. Discs of solid **2** that were left in the dissolution bath at 37°C for 24 h showed that after 24 h exposure to liquid water they had completed converted to **1** by XRPD.

In order to demonstrate the kinetics of phase transformation of **2** back to **1** in the presence of water, a humidity generator was attached to the XRPD sample stage. XRPD was performed on a sample of **2** after exposure to 100% RH water vapor at room temperature for 2, 6, and 24 h. Figure 9 shows the XRPD results after exposure of **2** to 100% RH. The cocrystal is stable to conversion through 6 h exposure to 100% RH. After 24 h exposure to 100% RH, the cocrystal converts to **1**.

The mean pharmacokinetic metrics calculated from the dog study data are summarized in Table II. The mean AUC values for the 5 mg/kg dose were 374 and 1,234 ng h/ml for **1** and **2**, respectively. At this low dose, use of the cocrystal significantly improved *in vivo* exposure in dogs (Welch ANOVA testing for equal means with unequal variances, $p = 0.0169$). At the 50 mg/kg dose, the AUC values were 889 and 2,230 ng h/ml for **1** and **2**, respectively. Statistically this difference in AUC values was also significant ($p = 0.0268$) as use of the cocrystal significantly improved exposure. The systemic exposure based on plasma AUC, increased with increasing oral dose; however, the exposure is not proportional to the dose. The Cmax metrics also show significantly improved exposures when **2** instead of **1** is used. Figures 10 and 11 show the plasma concentration profiles for **1** and **2** at both dosing levels.

Water sorption of **2** was determined at 25°C and the results are shown in Fig. 12. The cocrystal is considered nonhygroscopic as it sorbs less than 0.08% water even at high humidities (95% RH) through repeated sorption and desorption cycles. Samples of the cocrystal stored at 40°C/75% RH and 60°C for 2 months showed no change by XRPD and DSC, and HPLC impurity analyses did not show significant increases in any known degradants during storage. Although **2** is stable as an isolated solid, the tendency to convert to **1** when exposed to water is not a desirable property from a processing point of view, although in this case kinetic stability may be sufficient to allow standard processing steps to be used. The advantage of increased bioavailability that **2** provides must be considered relative to this potential processing disadvantage.

Recent research indicates that the phase solubility diagrams of cocrystals are affected by the concentration of each component in solution and the amount of solution complexation that occurs (33). These results suggest that a crystallization process for obtaining **2** may be partially controlled by manipulating the supersaturation levels of the individual components in the crystallization vessel. Continued research in this area may potentially shed light on the mechanisms that govern the dissolution of cocrystals compared to homomeric APIs once the thermodynamic factors relating homomeric and multi-component structures are also taken into consideration. In the case of the increased water

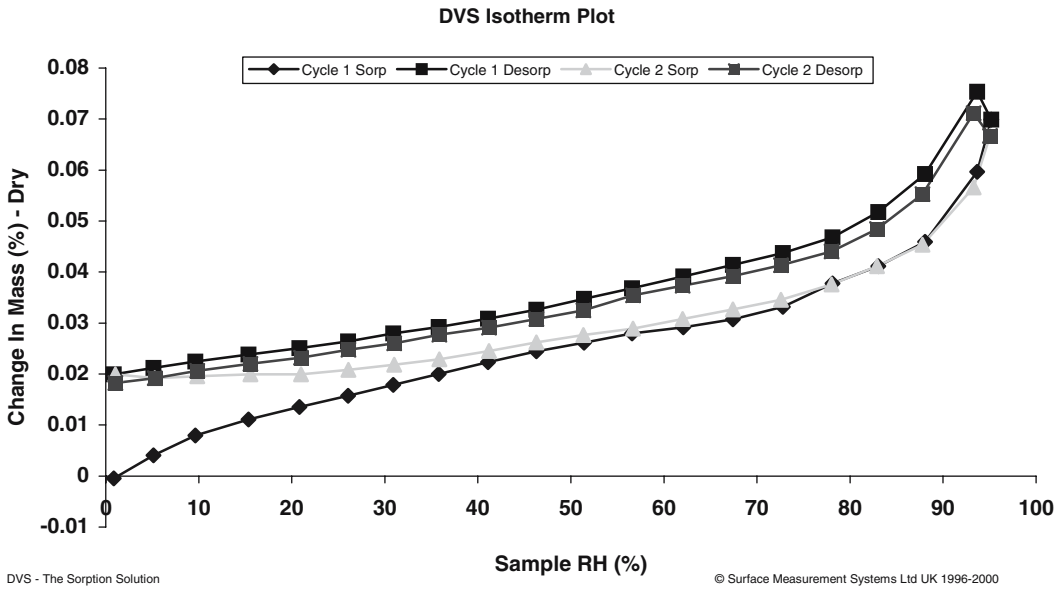

Fig. 12. Water sorption of **2** at 25°C, repeated sorption and desorption isotherms.

solubility of **2** compared to **1**, we presume that the lower thermal stability (indicating a lower lattice energy compared to **1**) and the higher water solubility of glutaric acid are the primary factors that contribute to the rapid dissolution of **2** in water.

Particle size characterization of the lots used in the pharmacokinetic studies showed that **1** had a smaller particle size than **2**. The volumetric median diameter ($D_v(0.5)$) comparison for **1** *versus* **2** is 24 and 49 μm, respectively, and the volumetric 90th percentile ($D_v(0.9)$ comparisons are 55 and 131 μm, respectively. From a particle size and surface area exposure perspective, the solids representing **1** had a distinct advantage compared to cocrystal solids used in the pharmacokinetic comparison as the smaller particles would be expected to have a faster *in vivo* dissolution rate.

CONCLUSION

Compound **1** is a low solubility compound with low *in vitro* dissolution characteristics and low *in vivo* plasma concentrations after oral dosing of the crystalline solid in dogs. As a suspected Class II BCS, the low dissolution rate, a direct consequence of **1**'s insolubility, was assumed to be the barrier to increased bioavailability rather than the permeability.

A cocrystal (**2**) incorporating **1** and glutaric acid was designed and generated in gram quantities. The intrinsic dissolution rate comparison between **1** and **2** showed that use of the cocrystal significantly increases the *in vitro* rate of delivery of **1** into the aqueous environment of the dissolution media. The AUC results from dog studies at both low dose (5 mg/kg) and high dose (50 mg/kg) uniquely confirms that the use of **2** does improve the *in vivo* bioavailability of the parent compound (**1**). The incidental delivery of glutaric acid is not expected to be an issue as glutaric acid is a normal component of foodstuffs and a metabolic intermediate. Cocrystal **2** is kinetically stable as an isolated crystalline solid and chemically and physically stable when stored under stress conditions of 40°C/75% RH and 60°C for 2 months.

The combination of lower thermal stability for **2** compared to **1** and the high water solubility of the glutaric acid guest molecule contribute to the 18 times increase in the dissolution rate in water for **2** compared to **1**. The increased dissolution rate of **2** translated into plasma concentration values that were nearly three times higher for **2** than **1** when dogs were dosed orally. These reported biological results demonstrate for the first time that use of a cocrystal (molecular complexes of non-ionizable drug with pharmaceutically acceptable guest compound) is a viable approach for increasing the bioavailability of drugs with low aqueous solubility.

ACKNOWLEDGMENTS

The authors thank Dr. Ken Hardcastle at the Emory University Chemistry Department X-Ray Diffraction Center for collecting and solving the single crystal structure of the cocrystal. The authors also acknowledge the support of Drs. Phil Goliber and Leah Lipsich of Purdue Pharma L. P.

REFERENCES

1. G. L. Amidon, H. Lennernas, V. P. Shah, and J. R. Crison. A theoretical basis for biopharmaceutic drug classification: the correlation of *in vitro* drug product dissolution and *in vivo* bioavailability. *Pharm. Res.* **12**:413–419 (1995).
2. Calculated using Advanced Chemistry Development (ACD/Labs) Software Solaris V4.67 (1994–2005 ACD/Labs).
3. M. Yazdanian, S. L. Glynn, J. L. Wright, and A. Hawi. Correlating partitioning and Caco-2 cell permeability of structurally diverse small molecular weight compounds. *Pharm. Res.***15**(9):1490–1494 (1998).
4. S. L. Childs, L. C. Chyall, J. T. Dunlap, V. N. Smolenskaya, B. C. Stahly, and G. P. Stahly. Crystal engineering approach to forming cocrystals of amine hydrochlorides with organic acids. Molecular complexes of fluoexetine hydrochloride with benzoic, succinic, and fumaric acids. *J. Am. Chem. Soc.* **126**:13335–13342 (2004).
5. J. F. Remenar, S. L. Morissette, M. L. Peterson, B. Moulton, J. M. MacPhee, H. R. Guzman, and O. Almarsson. Crystal engineering of novel cocrystals of a triazole drug with 1,4-dicarboxylic acids. *J. Am. Chem. Soc.* **125**:8456–8457 (2003).
6. J. W. Bettis, J. L. Lach, and J. Hood. Effect of complexation with phenobarbital on biologic availability of theophylline from 3 tablet formulations. *Am. J. Hosp. Pharm.* **30**(3):240–243 (1973).
7. J. Bernstein, M. C. Etter, and L. Leiserowitz. The role of hydrogen bonding in molecular assemblies. In H.-B. D. Buergi and D. Jack (eds.), *Struct. Correl.*, VCH, Weinheim, Germany, 1994, pp. 431–507.
8. I. D. H. Oswald, D. R. Allan, P. A. McGregor, W. D. S. Motherwell, S. Parsons, and C. R. Pulham. The formation of paracetamol (acetaminophen) adducts with hydrogen-bond acceptors. *Acta Crystallogr. Sect. B-Struct. Commun.* **58**:1057–1066 (2002).
9. N. Sardone, G. Bettinetti, and M. Sorrenti. Trimethoprim-sulfadimidine 1:2 molecular complex monohydrate. *Acta Crystallogr., Sect. C Cryst. Struct. Commun.* **53**:1295–1299 (1997).
10. S. Nakao, S. Fujii, T. Sakaki, and K. I. Tomita. Crystal and molecular-structure of 2-1 molecular-complex of theophylline with phenobarbital. *Acta Crystallogr. Sect. B-Struct. Commun.* **33**:(MAY 13) (1977).
11. M. R. Caira, T. G. Dekker, and W. Liebenberg. Structure of a 1:1 complex between the anthelmintic drug mebendazole and propionic acid. *J. Chem. Crystallogr.* **28**(1):11–15 (1998).
12. M. C. Etter and G. M. Frankenbach. Hydrogen-bond directed cocrystallization as a tool for designing acentric organic solids. *Chem. Mater.* **1**(1):10–12 (1989).
13. C. B. Aakeroy. Crystal engineering: strategies and architectures. *Acta Crystallogr. Sect. B-Struct. Commun.* **53**:569–586 (1997).
14. M. C. Etter and D. A. Adsmond. The use of cocrystallization as a method of studying hydrogen-bond preferences of 2-aminopyrimidine. *J. Chem. Soc., Chem. Commun.* **8**:589–591 (1990).
15. G. R. Desiraju. Supramolecular synthons in crystal engineering—a new organic-synthesis. *Angew. Chem.-Int. Edit. Engl.* **34**(21):2311–2327 (1995).
16. A. Nangia and G. R. Desiraju. Supramolecular structures —reason and imagination. *Acta Crystallogr. Sect. A* **54**:934–944 (1998).
17. B. Rodriguez-Spong, C. P. Price, A. Jayasankar, A. J. Matzger, and N. Rodriguez-Hornedo. General principles of pharmaceutical solid polymorphism: a supramolecular perspective. *Adv. Drug Deliv. Rev.* **56**(3):241–274 (2004).
18. J. J. Kane, T. Nguyen, J. Xiao, F. W. Fowler, and J. W. Lauher. The host guest co-crystal approach to supramolecular structure. *Mol. Cryst. Liquid Cryst.* **356**:449–458 (2001).
19. P. Vishweshwar, A. Nangia, and V. M. Lynch. Molecular complexes of homologous alkanedicarboxylic acids with isonicotinamide: X-ray crystal structures, hydrogen bond synthons, and melting point alternation. *Cryst. Growth Des.* **3**(5):783–790 (2003).
20. P. Vishweshwar, A. Nangia, and V. M. Lynch. Supramolecular synthons in phenol-isonicotinamide adducts. *Crystengcomm.*: 164–168 (2003).
21. M. C. Etter. Aggregate structures of carboxylic acids and amides. *Isr. J. Chem.* **25**(3–4):312–319 (1985).
22. SMART Version 5.55, 2000, Bruker AXS, Inc., Analytical X-ray Systems, 5465 East Cheryl Parkway, Madison Wisconsin 53711–5373.
23. SAINT Version 6.02, 1999, Bruker AXS, Inc., Analytical X-ray

Systems, 5465 East Cheryl Parkway, Madison Wisconsin 53711–5373.
24. SHELXTL V5.10, 1997, Bruker AXS, Inc., Analytical X-ray Systems, 5465 East Cheryl Parkway, Madison Wisconsin 53711–5373.
25. A. J. C. Wilson (ed.), *International Tables for X-ray Crystallography, Volume C.* Kynoch, Academic, Dordrecht, **1992**, Tables 6.1.1.4 (pp. 500–502) and 4.2.6.8 (pp. 219–222).
26. C. G. S. Wermuth. P. H. Handbook of Pharmaceutical Salts; Properties, Selection, and Use (P. H. W. Stahl, C. G., ed.). Verlag Helvitica Chimica Acta, Zurich and Wiley-VCH: Weinheim, 306 (2002).
27. W. C. McCrone Jr. *Fusion Methods in Chemical Microscopy*, Interscience, New York, 1957.
28. A. Kofler. Behavior of crystalline solid solution during melting and crystallization. *Mikroskopie.* **11**(5–6):140–155 (1956).
29. M. Kunhert-Brandstaetter. 40 Years of Kofler methods. *Pharma Int. (Engl. Ed.)* **5**:5–11 (1971).
30. R. N. Rai and K. B. R. Varma. Phase diagram and dielectric studies of binary organic materials. *Mater. Lett.* **44**(5):284–293 (2000).
31. U. S. Rai and S. George. Some thermochemical studies on binary faceted organic eutectics and 1:1 molecular complexes. *J. Therm. Anal.* **46**(6):1809–1820 (1996).
32. N. R. Jagannathan and C. N. R. Rao. A ^{13}C NMR spectroscopic study of the phase transitions of alkane dicarboxylic acids in the solid state. *Chem. Phys. Lett.* **140**(1):46–50 (1987).
33. S. J. Nehm, B. Rodriguez-Spong, and N. Rodriguez-Hornedo. Phase solubility diagrams of cocrystals are explained by solubility product and solution complexation. *Cryst. Growth Des.* **6**(2):592–600 (2006).